Basic Relations for Relativistic Beams, I

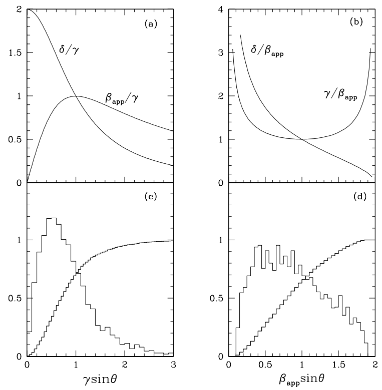

Curves for $\gamma^2 \gg 1$ (Cohen et al., 2007)

Remember standard relations for ideal relativistic beams:

$$\delta = \frac{1}{\gamma(1-\beta\cos\theta)} \quad (6.35)$$

$$\beta_{\rm app} = \frac{\beta\sin\theta}{1-\beta\cos\theta} \quad (6.36)$$

and

$$L = L_0 \mathcal{D}^{p-\alpha} \quad . \quad (6.37)$$

$p-\alpha$ depends on the jet geometry (e.g., $p = 2$ for a smooth series of blobs or $p = 3$ for a single isolated blob; Lind & Blandford, 1985).

If $\sin\theta = \gamma^{-1}$, $\mathcal{D} = \gamma$ and $\beta_{\rm app} = \beta_{\rm app,max} = \beta\gamma$!

From Eq. 6.38 and Eq. 6.39, any two of the four parameters $\beta_{\rm app}, \gamma, \mathcal{D}$, and θ can be used to find the others!

Basic Relations for Relativistic Beams, II

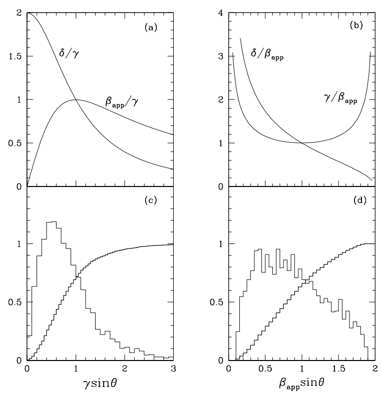

Curves for $\gamma^2 \gg 1$ (Cohen et al., 2007)

Remember standard relations for ideal relativistic beams:

$$\delta = \frac{1}{\gamma(1-\beta\cos\theta)} \quad (6.38)$$

$$\beta_{\rm app} = \frac{\beta\sin\theta}{1-\beta\cos\theta} \quad (6.39)$$

and

$$L = L_0 \mathcal{D}^{p-\alpha} \quad . \quad (6.40)$$

$p-\alpha$ depends on the jet geometry (e.g., $p = 2$ for a smooth series of blobs or $p = 3$ for a single isolated blob; Lind & Blandford, 1985).

If $\sin\theta = \gamma^{-1}$, $\mathcal{D} = \gamma$ and $\beta_{\rm app} = \beta_{\rm app,max} = \beta\gamma$!

Define the critical angle θ_c so that $\sin\theta_c = \gamma^{-1}$: $\theta/\theta_c \sim \gamma\sin\theta$ (accurate for $\gamma^2 \gg 1$ and $\theta \ll 1$) and still correct to 20 % for $\beta > 0.5$ and $\theta < 60°$.

Monte-Carlo Simulations of a Jet Sample, I

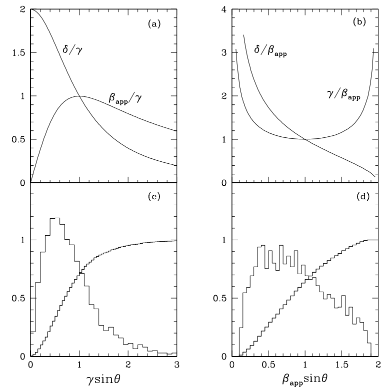

Curves for $\gamma^2 \gg 1$ (Cohen et al., 2007)

Because $S_\nu \propto \mathcal{D}^2$ (for $\alpha \sim 0$), and because $\mathcal{D}$ decreases with increasing θ, the sources found in a flux-density limited sample will preferantially be at small angles, even though there is not much solid angle there.

Problem: $p(\theta|\beta_{\rm app,f})$ is not an anlytical function. ⇒ use Monte-Carlo simulations to study the probability funtions.

- Peak of the probability distribution at $\gamma\sin\theta = \theta/\theta_c = 0.6$. At this position, $\beta_{\rm app} = 0.9\gamma$ and $\mathcal{D} = 1.5\gamma$.
- 50 % point of $P(\theta|\gamma_{\rm f})$ is at $\gamma\sin\theta = \theta/\theta_c = 0.7$.
- About 75 % of all sources lie inside their $1/\gamma$ cones!

Almost all sources (0.04 $< P <$ 0.96) lie within the range $0.15\theta_c - 2\theta_c$!

Monte-Carlo Simulations of a Jet Sample, II

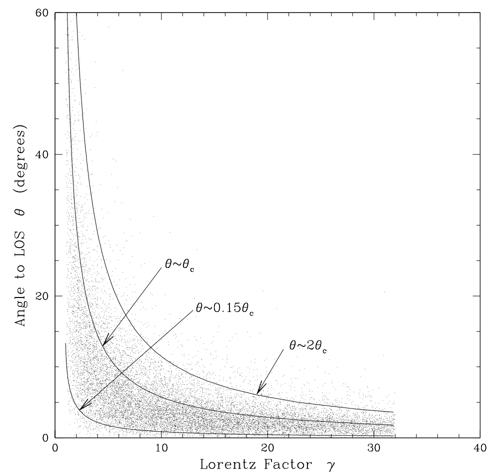

Distribution of 14000 sources selected randomly from a Monte-Carlo simulated parent population of jets (Cohen et al., 2007).

Input for the M-C simulation was a parent population with a power-law distribution of Lorentz factors with index −1.25 and peak $\gamma = 32$ and a power-law distribution of intrinsic luminosities with index −2.73 and minimum luminosity 1×10^{24} W Hz^{-1} (fits the MOJAVE data; see below).

Monte-Carlo Simulations of a Jet Sample, III

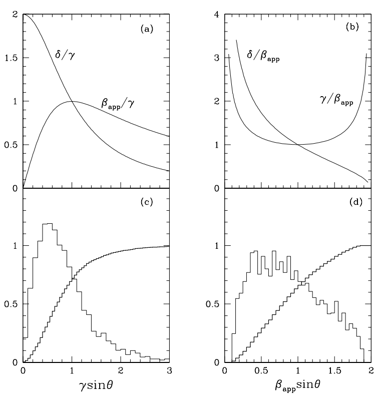

Curves for $\gamma^2 \gg 1$ (Cohen et al., 2007)

We have described $p(\theta|\gamma_f)$, but we do observe β_{app} and not γ. What is the probability of finding a jet at the angle θ if it shows apparent superluminal motion with $\beta_{app,f}$?

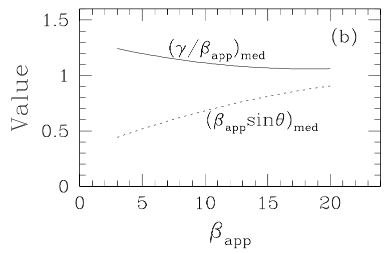

The probability density curve for $p(\theta|\beta_{app,f})$ is broad and as β_{app} decreases, it becomes more peaked and the peak shifts to smaller values.

Monte-Carlo Simulations of a Jet Sample, IV

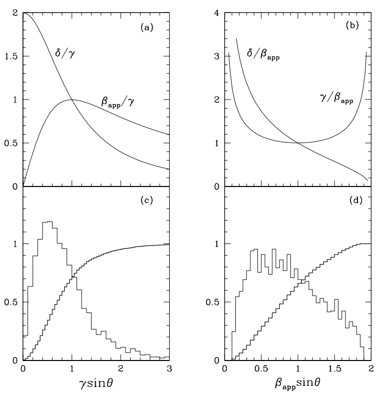

Curves for $\gamma^2 \gg 1$ (Cohen et al., 2007)

Now, what is the probability of finding a jet with a Lorentz factor γ if it shows apparent superluminal motion with $\beta_{app,f}$?

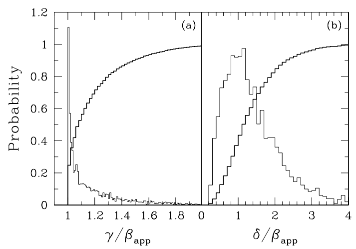

The probability density curve for $p(\gamma|\beta_{app,f})$ is sharply peaked at $\gamma \sim \beta_{app}$.

For about half the sources with $\beta_{app} \sim 15$, γ lies between 15 and 16, but the other half is distributed to the highest Lorentz factors in the parent distribution!

Monte-Carlo Simulations of a Jet Sample, V

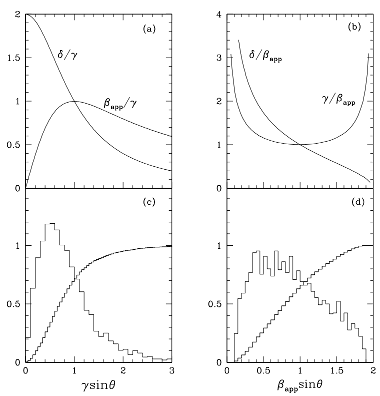

Curves for $\gamma^2 \gg 1$ (Cohen et al., 2007)

Finally, what is the probability of finding a jet with a Doppler factor $\mathcal{D}$ if it shows apparent superluminal motion with $\beta_{app,f}$?

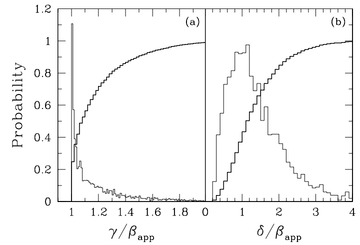

The probability density curve for $p(\mathcal{D}|\beta_{app,f})$ doesn't have a sharp peak.

The intrinsic luminosity L_0, which scales as $\mathcal{D}^2$, is only poorly constrained by the measured superluminal motion.

The Inversion Problem, I

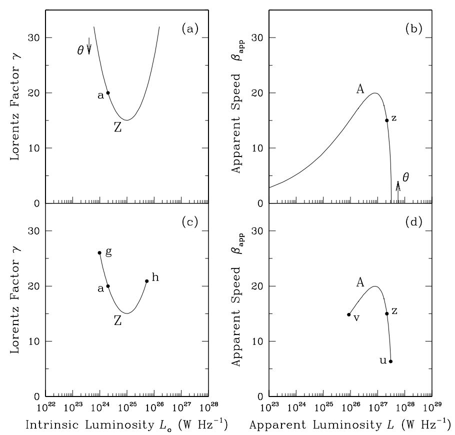

Consider a source at point **a** in the intrinsic plane, with $\gamma = 20$ and $L_0 = 2 \times 10^{24}$ W Hz^{-1}. Let it be observed at $\theta = 1.3°$, so that $\beta_{app} = 15.0$ and $L = 2.2 \times 10^{27}$ W Hz^{-1}. This is point **z** in the observation plane.

Now let θ vary and the observables for source **a** will follow the aspect curve **A**. The aspect curve shows all possible observable (β_{app}, L) pairs for a given source **a**.

The height of the aspect curve is fixed by γ. The position on the x-axis is determined by both γ and L_0. The width of the peak is controlled by the exponent p $(L = L_0\mathcal{D}^{p-\alpha})$.

The Inversion Problem, II

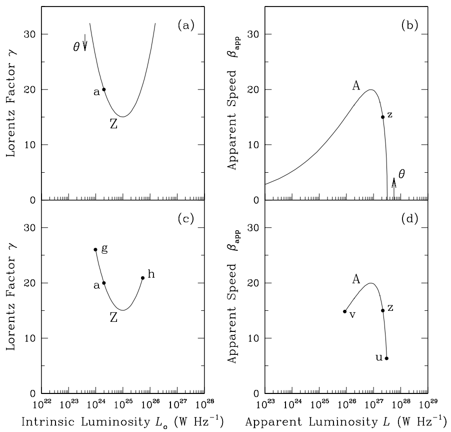

Now, consider a source at point **z** in the observation plane, with $\beta = 15$ and $L = 2.2 \times 10^{27}\,\mathrm{W\,Hz^{-1}}$.

Curve **Z** in the intrinsic plane describes all possible pairs of intrinsic parameters (γ, L_0), which could produce source **z** (under the appropriate viewing angle θ). **Z** is called the origin curve.

The inversion for the observed source **z** is not unique. Any point on the origin curve **Z** could be its counterpart as θ can vary from 0° to 90°. This gives only broad limits to γ and L_0.

The Inversion Problem, III

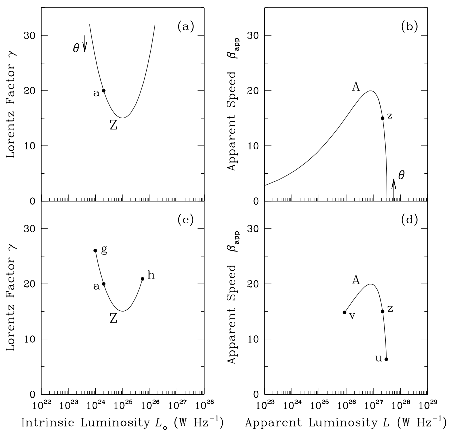

(Cohen et al., 2007)

We found: almost all sources $(0.04 < P < 0.96)$ lie within the range $0.15\theta_c - 2\theta_c$!

I.e., we can truncate the origin curve for point **z** in the intrinsic plane at $P(\gamma|\beta_{\mathrm{app,f}}) = 4\,\%$ and at 96 %. Similarly, the aspect curve for source **a** in the observation plane can be cut at $P(\theta|\gamma_f) = 4\,\%$ and at 96 %.

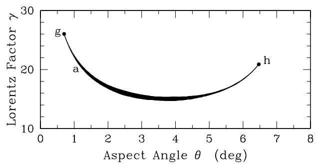

Probablistic limits for the intrinsic parameters of source **z**: $15 < \gamma < 26$ and $1 \times 10^{24}\mathrm{W\,Hz^{-1}} < L_0 < 5 \times 10^{25}\mathrm{W\,Hz^{-1}}$.

Caveats

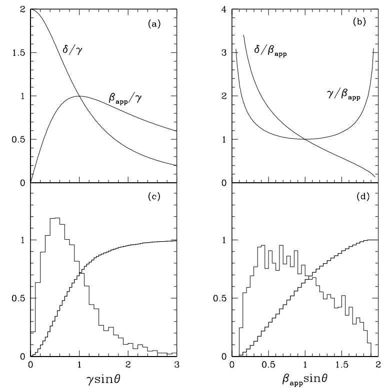

Curves for $\gamma^2 \gg 1$ (Cohen et al., 2007)

WYSIWYB Assumption:
$\gamma_p = \gamma_b$ ("What You See Is What You Beamed")

This is NOT trivial! You assume that the core and jet-beam plasma is beamed with the same Doppler factor as the moving blob pattern.
It is even less trivial, whether or not the high-energy emission (X-rays, γ-rays) are beamed with the same Doppler factor.

Additional complication: the same jet can have VLBI components with different speeds (e.g., standing shocks, trailing components, etc... Agudo et al., 2001).

Superluminal Motion Statistics, I

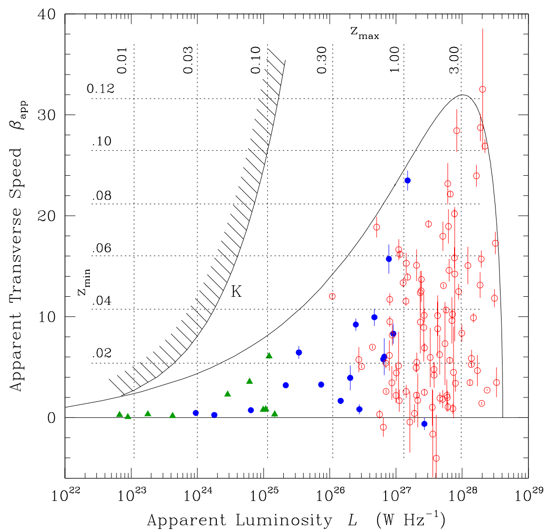

(Cohen et al., 2007)

Application of these results to MOJAVE data:

- Measured jet speeds β_{app} and radio (VLBI) luminosities L for 119 sources (Cohen et al., 2007)
- An aspect curve for $\gamma = 32$ and $L = 10^{25}\,\mathrm{W\,Hz^{-1}}$ forms an **envelope** to all data
- $\Rightarrow$ there is an upper limit to both distributions of γ and L!
- No high-β_{app}, low-L sources
- Selection effect because of flux-density and detectable-speed limits?

Superluminal Motion Statistics, II

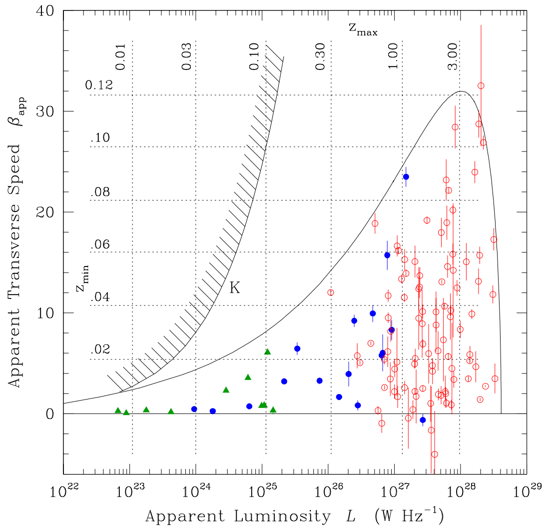

(Cohen et al., 2007)

- Observation epochs typically separated by 1 year. This limits the maximum detectable angular motion μ_{max} to $\sim$ 4 mas yr^{-1}.
- Sources weaker than 500 mJy were typically not included in the survey.
- $\Rightarrow$ Sources left of curve **K** are inaccessible to MOJAVE
- Every point (β_{app}, L) to the right of curve **K** and left of the envelope has a range of redshift within which it would be observable, i.e., MOJAVE measured a spatial volume free of such sources.

$\Rightarrow$ The lack of luminous slow sources is not a selection effect!

Superluminal Motion Statistics, III

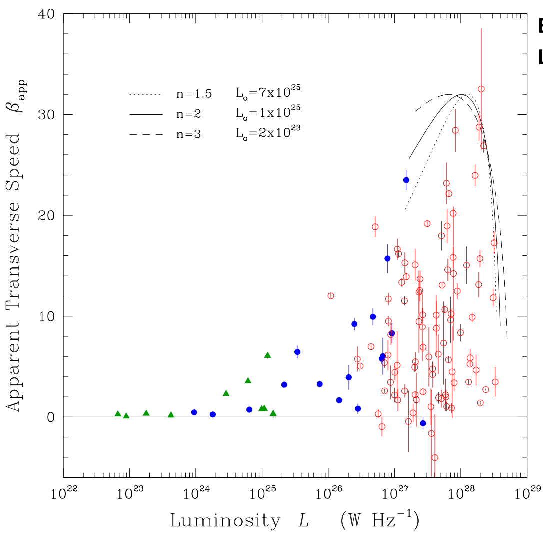

(Cohen et al., 2007)

Boost Exponent and Maximum Lorentz Factor:

- The boost exponent p from Eq. 6.40 controls the sharpness of the peak
- $n = 3$ can fit the data only if the strong distant quasars near the peak have intrinsic luminosities L_0 comparable to the weak jets in nearby galaxies.
- We saw that the probability of selecting a source $p(\theta|\beta_{app,f})$ is maximized near $\theta = 0.6\theta_c$, where $\beta_{app} \sim 0.9\gamma$.

$\Rightarrow$ $\beta_{app,max} \sim 32$ implies $\gamma_{max} \sim 32$!

Superluminal Motion Statistics, IV

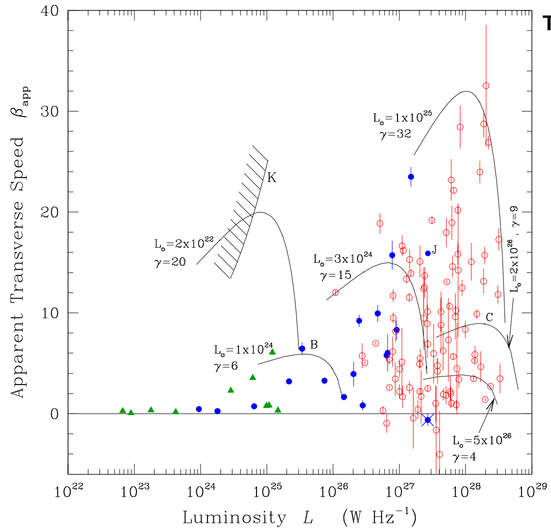

(Cohen et al., 2007)

The Distribution of γ and L_0:

- β_{app} and L are correlated: fast superluminal motion occurs only in very luminous sources; moderate superluminal motion is found in all luminosity classes.
- $\Rightarrow$ There must be a similar correlation between γ and L_0.
- Each individual source is quite likely to lie near the peak of an aspect curve and very likely between the 4 % and 96 % probability cutoff.

The envelope can be understood as a series of aspect curves with successively lower values of γ.

Superluminal Motion Statistics, V

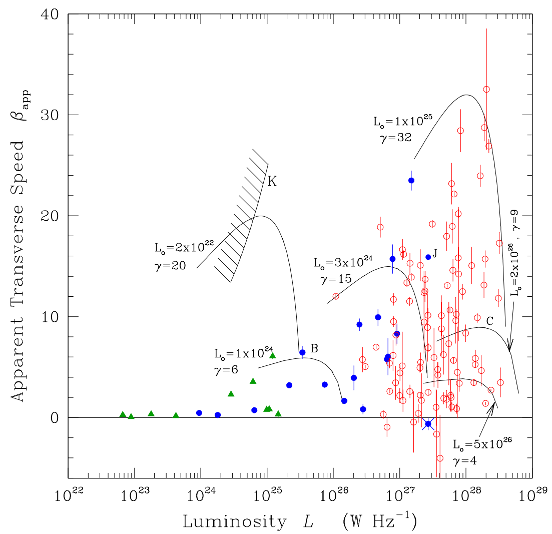

(Cohen et al., 2007)

- Consider the BL Lac object **B**: it could belong to either the $\gamma = 6$ or the $\gamma = 20$ aspect curve.
- But if it belongs to the low-probability region of the $\gamma = 20$ aspect curve, where are all the sources of this population closer to the high-probability region?
- Alternatively, source **B** could be a high-angle version of the sources near the peak of the $\gamma = 15$ curve. But the probability for that is $\ll 4$ %.

The galaxies and BL Lac objects in the lower left part of the distribution are not off-axis versions of the powerful quasars, nor are they high-γ, low-L_0 sources!

Superluminal Motion Statistics, VI

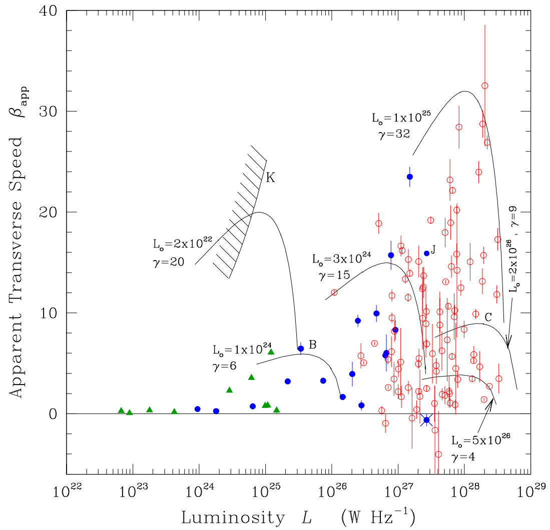

(Cohen et al., 2007)

- Source **B** is actually BL Lac itself.
- A detailed study (Denn, Mutel & Marscher, 2000) showed that for this particular object $\theta = 9^\circ \pm 2^\circ$; combined with the measured speed $\beta_{app} = 6.6 \pm 0.6$, it follows that $\gamma = 7 \pm 1$.

Superluminal Motion Statistics, VII

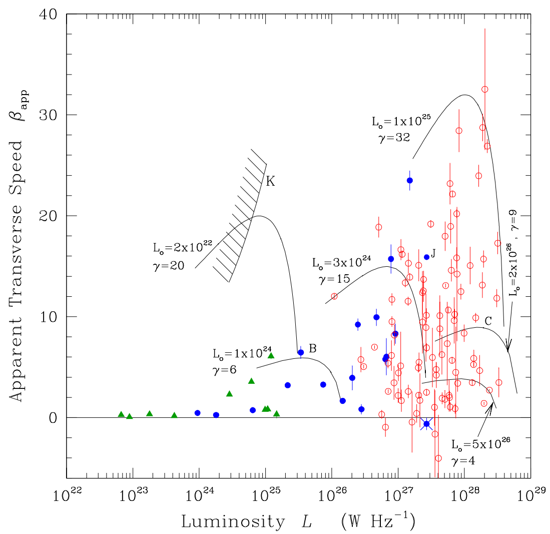

(Cohen et al., 2007)

- Now, consider the many quasars near point **C**: some of them may belong to the $\gamma = 9$, $L_0 = 2 \times 10^{26}$ W Hz $^{-1}$ curve, but that is about as far to the right as should be considered (no sources near the peaks of the higher-luminosity curves).
- Unless one assumes a negative correlation between γ and L_0, some of the sources near point **C** should have values of $\gamma = 20$ or more (at appropriately small angles).

$\Rightarrow$ The distribution of L_0 may extend up to 10^{26} W Hz^{-1}.

Superluminal Motion Statistics, VIII

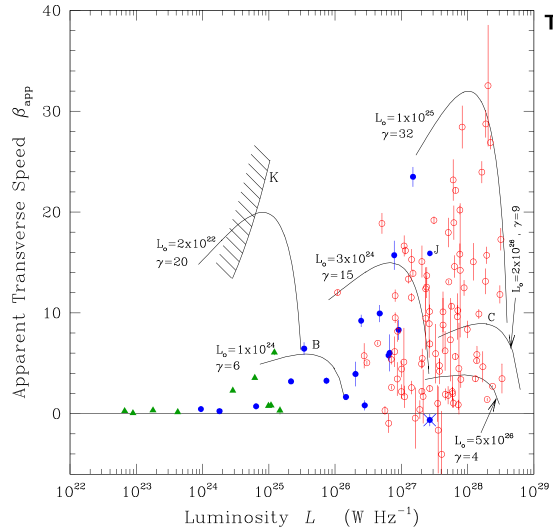

(Cohen et al., 2007)

The Slow Quasars and BL Lacs:

- 25 out of 105 powerful ($L > 3 \times 10^{25}$ W Hz^{-1}) quasars and BL Lac objects have $\beta_{app} < 3$. $\Rightarrow$ low probability if $\gamma > 10$.
- Options:
  1. End-on viewed high-γ sources: unlikely!
  2. Low-γ, high-L_0 sources: unlikely (see discussion of point **C**)!

Many of the slow quasars and BL Lacs may have $\gamma_p < \gamma_b$!

WYSMNBWYB!

Superluminal Motion Statistics, IX

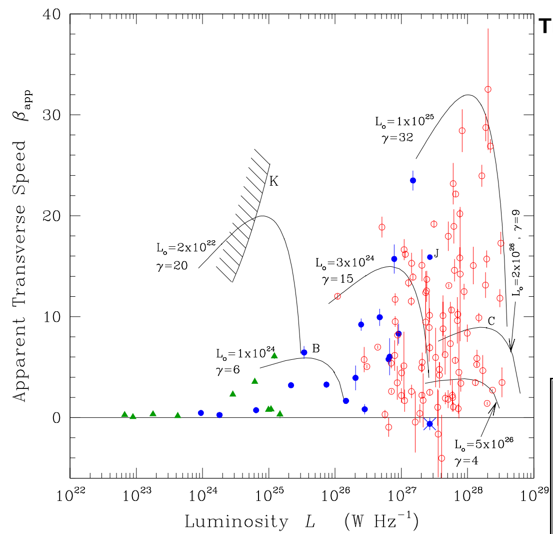

(Cohen et al., 2007)

The Fast Galaxies:

- Only 3 superluminal galaxies: all broad-emission line radio galaxies.
- $\theta < 2 \arctan \beta_{app}^{-1} \sim 20^\circ - 45^\circ$ (from Eq. 6.39).
- From external variability data, the Doppler factors for these three sources can be estimated, leading to values of $\gamma = 4 - 7$ and $L_0 = 10^{23} - 10^{24}$ W Hz^{-1}.

The Lorentz factors of the superluminal galaxies are similar to those of the slower quasars. But their intrinsic luminositeis do not overlap. They represent different populations!

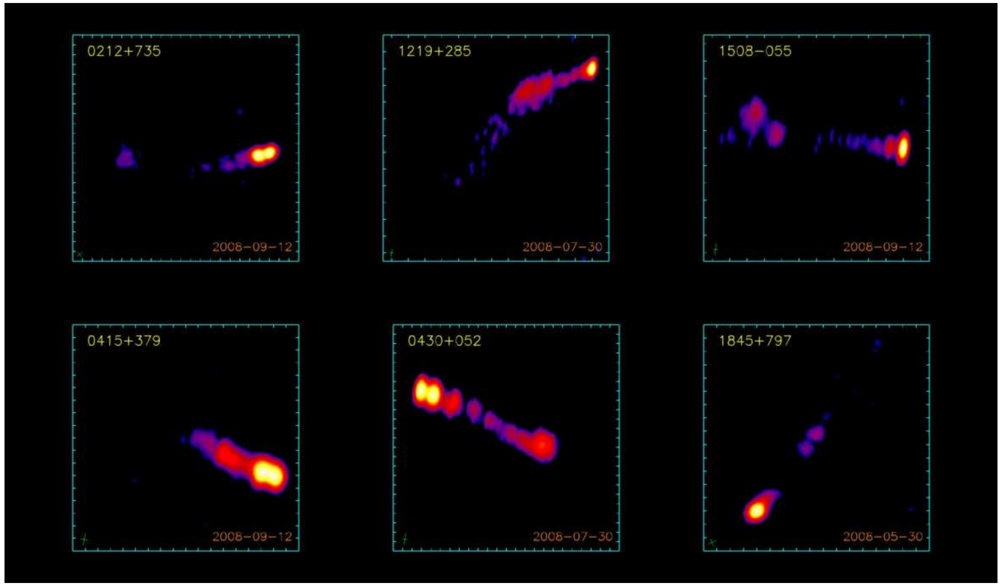

Morphology and kinematics of slow quasars and fast galaxies very similar.
But different populations!

Superluminal Motion Statistics, XI

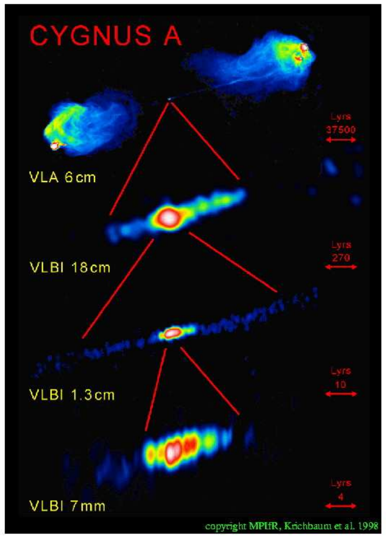

Image MPIfR

A special Case: Cygnus A

- Measured speed: $\beta_{\text{app}} = 0.83 \pm 0.12$ (subluminal)
- Angle to the line of sight: $45^\circ < \theta < 70^\circ$
- Lorentz factor: $1.24 < \gamma < 1.36$
- Jet speed: $0.59 < \beta < 0.68$ (only mildly relativistic)
- But the powerful lobes and hotspots indicate highly relativistic plasma

This apparent contradiction is solved, if the jets are assumed to have a stratified structure of at least two components: a highly relativistic spine and a mildly relativistic sheath.

In this model, Cygnus A is so exceptional, because it is accidentally nearby. If it were at $z \sim 1$ and pointed near the line of sight, it would be a normal quasar.

Other VLBI Jet Surveys

VLBA Imaging and Polarimetry Survey (VIPS): combined 5 GHz and 15 GHz survey of 1100 AGN with full polarization (Helmboldt et al., 2008; Taylor et al., 2007)

Flux-density limit about an order of magnitude below MOJAVE but no monitoring

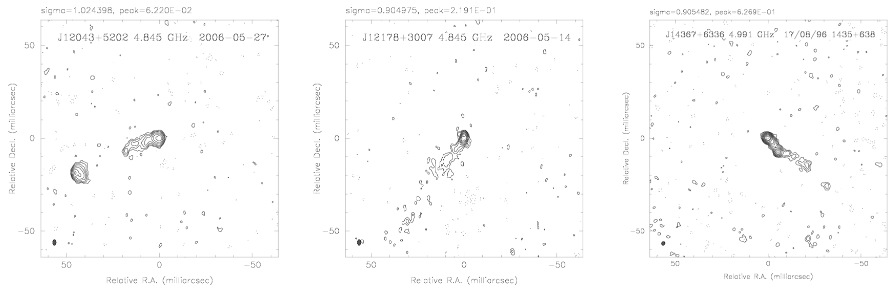

http://www.phys.unm.edu/~gbtaylor/VIPS/

Other VLBI Jet Surveys

Other VLBI surveys:

- Pearson-Readhead Survey (Pearson & Readhead, 1981, 1988): first large VLBI jet survey (65 objects)
- Caltech-Jodrell Bank 1/2 Surveys (Polatidis et al., 1995; Thakkar et al., 1995; Xu et al., 1995): in combination with PR, first (sort of) complete flux-density limited sample; observed at 5 GHz and 1.6 GHz
- VCS (VLBA Calibrator Survey `http://www.vlba.nrao.edu/astro/calib/`): huge database to find calibrators for VLBI observations (but also snapshot images)
- RRFID (Radio Reference Frame Image Database `http://rorf.usno.navy.mil/rrfid.shtml`): motivated by astrometric precision studies (waive sources with too much structure)

Introduction, I

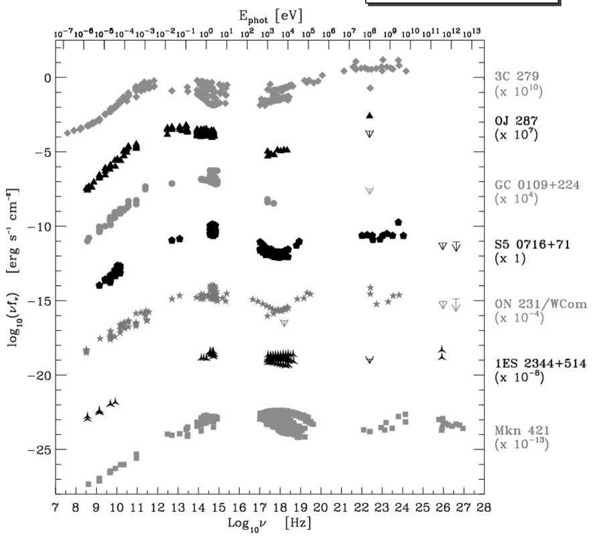

Radio-loud AGN emit across the whole electromagnetic spectrum!

This holds for the compact and large-scale jets of both quasars and radio galaxies.

How can we transfer the power of the compact jet into high-energy emission?

Sneak-preview of next week: a "blazar sequence" (Fiorucci, Ciprini & Tosti, 2004)

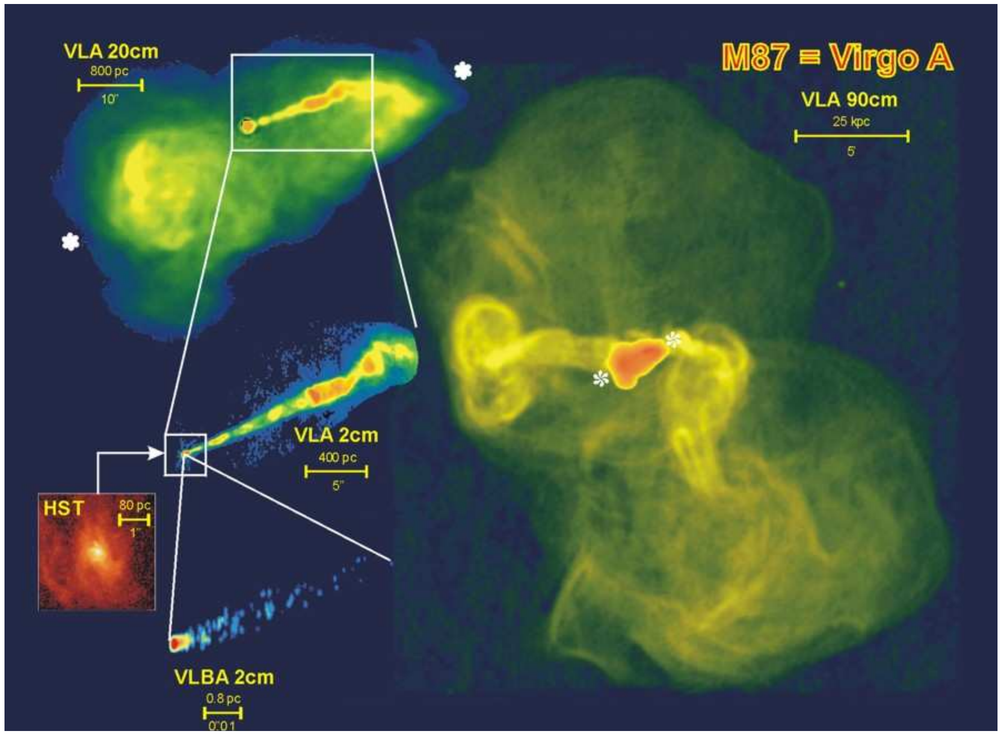

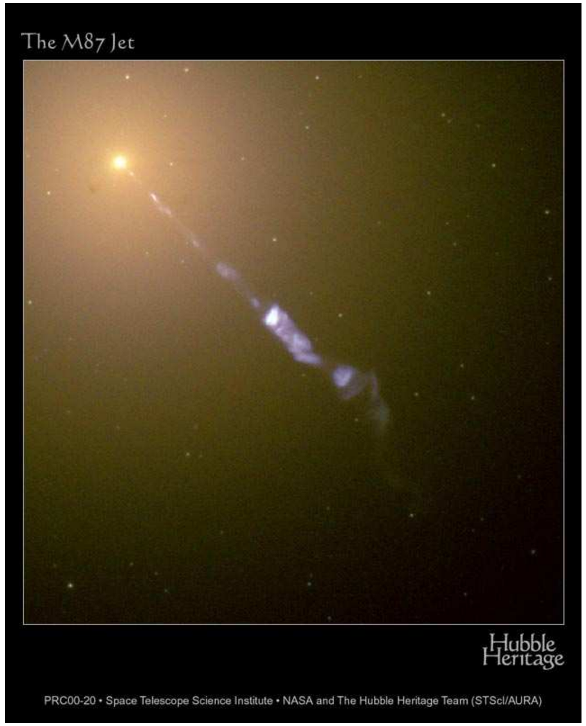

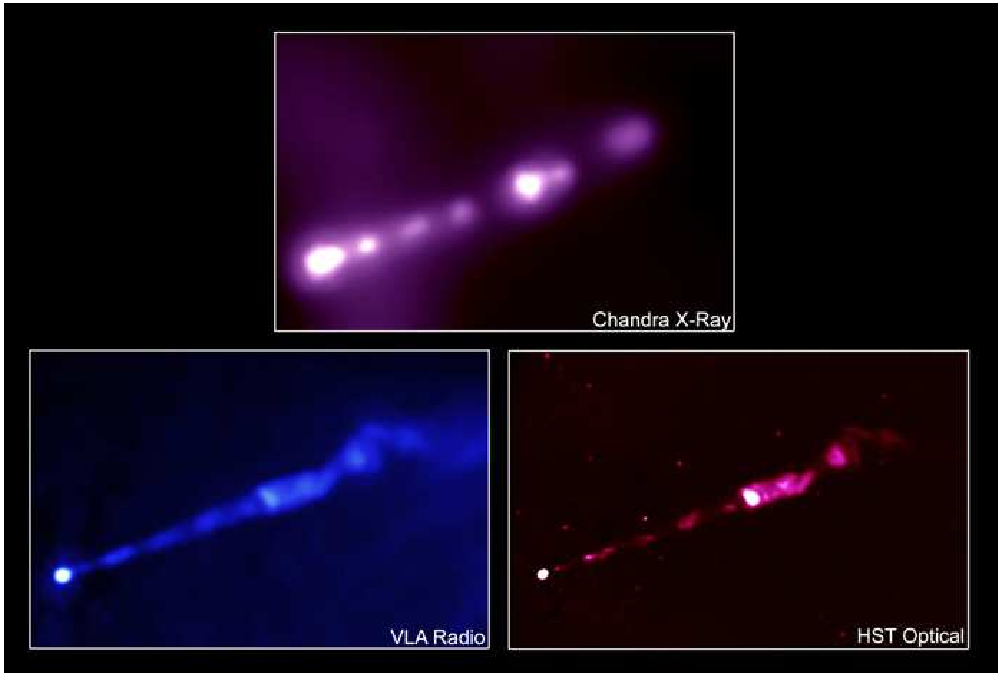

Introduction, VI

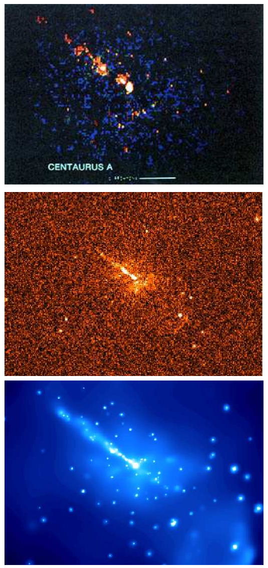

First imaging X-ray observations of jets with *Einstein* (1978-81)
Later *ROSAT* (1990-99)
Golden Era: *Chandra* (1999-present)
Now, $\sim$ 50 X-ray jets known.

Top: *Einstein*: Smithsonian Institution Photo No. 80-16249
Middle: *ROSAT*:
`http://www.mpe.mpg.de/Highlights/FB1997/h97-2-12.ps`
Bottom: *Chandra*: Chandra press release 2001-11-23

Visit the X-Jet homepage:
`http://hea-www.harvard.edu/XJET/`

X-ray Jet Surveys

Two major surveys conducted with *Chandra*:

- Sambruna et al. (2004): *A Survey of Extended Radio Jets with Chandra and the Hubble Space Telescope*
- Marshall et al. (2005): *A Chandra Survey of Quasar Jets: First Results*

Results: X-ray jets are common in beamed sources with large-scale radio jets (10/17 detections in Sambruna et al. (2004) and 16/19 in Marshall et al. (2005). Detectable with *Chandra* in 5 ksec snapshot observations.)

Both samples were selected to include known bright large-scale radio jets. About the same detection rate results from the analysis of the *Chandra*-observed MOJAVE sources, which are selected based on bright, beamed, compact jet emission (and admittedly on the research interests of *Chandra* proposers).

Inverse-Compton Emission, I

Most important process besides synchrotron emission:

Comptonization: Upscattering of low-energy photons by inverse Compton collisions off high-energy electrons.

Astronomically important in

- galactic black hole candidates
- active galactic nuclei: blazars, large-scale jets

Strategy: Refer to literature and the special lecture on radiative processes for details. Summarize main results, here.

Literature:

Blumenthal & Gould 1970, RMP 42, 237

Górecki & Wilczewski 1984, Acta Astron. 34, 141

Hua & Titarchuk 1995, ApJ 449, 188

Pozdnyakov et al. 1983, Astrophys. Rep. 2, 189

Sunyaev & Titarchuk 1980, A&A 86, 121

Inverse-Compton Emission, II

In relativistic jets, high-energy electrons are all around.

Physical process: Inverse Compton Scattering

Seed photons from

- the primary synchrotron photons of the jet emission: SSC – Synchrotron Self Compton emission (compact jets)
- an external photon field: EC – External Compton emission, e.g., from the cosmic microwave background (IC/CMB models: large-scale jet knots)

The most pressing problem in the context of large-scale extragalactic X-ray jets is whether or not the IC/CMB process is the dominant for high-power FR II and quasar jets or if (modified) synchrotron models can explain the observations.

Inverse-Compton Emission, III

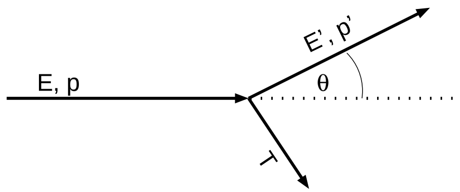

Electron–Photon Scattering:
$\Longrightarrow$ Photon changes direction and gains energy!
$\Longrightarrow$ Compton scattering.

Energy/wavelength change:

$$E' = \frac{E}{1 + \frac{E}{m_e c^2}(1 - \cos\theta)} \sim E\left(1 - \frac{E}{m_e c^2}(1 - \cos\theta)\right) \qquad (6.41)$$

and

$$\lambda' - \lambda = \frac{h}{m_e c}(1 - \cos\theta) \qquad (6.42)$$

where $h/m_e c = 2.426 \times 10^{-10}$ cm (Compton wavelength).

Averaging over θ, for $E \ll m_e c^2$:

$$\frac{\Delta E}{E} \approx -\frac{E}{m_e c^2} \quad . \qquad (6.43)$$

Inverse-Compton Emission, IV

For relativistic, non-stationary electrons, use previous formulae and Lorentz transform photon into electron's frame of rest (FoR):

1. Lab system $\Rightarrow$ electron's frame of rest:
$$E_{\text{FoR}} = E_{\text{Lab}}\gamma(1 - \beta\cos\theta) \qquad (6.44)$$
2. Scattering occurs, gives E'_{FoR}.
3. Electron's frame of rest $\Rightarrow$ Lab system:
$$E'_{\text{Lab}} = E'_{\text{FoR}}\gamma(1 + \beta\cos\theta') \qquad (6.45)$$

Therefore, if electron is relativistic:

$$E'_{\text{Lab}} \sim \gamma^2 E_{\text{Lab}} \qquad (6.46)$$

since (on average) θ, θ' are $\mathcal{O}(\pi/2)$.

Thus: Energy transfer is *very* efficient. Spectrum is "mirrored".

Inverse-Compton Emission, V

It can be shown that the net power gain of the photon field is

$$P_{\text{compt}} = \frac{4}{3}\sigma_T c\gamma^2\beta^2 U_{\text{rad}} \qquad (6.47)$$

Power emitted by synchrotron radiation in a B-field of energy density U_B was

$$P_{\text{synch}} = \frac{4}{3}\sigma_T c\gamma^2\beta^2 U_B \qquad (6.6)$$

Magnetized plasma: synchrotron photons are inverse Compton scattered by the electrons. Ratio of emitted powers:

$$\frac{P_{\text{compt}}}{P_{\text{synch}}} = \frac{U_{\text{rad}}}{U_B} \qquad (6.48)$$

Consequence of the fact that (in QED) synchrotron radiation is inverse Compton scattering off virtual photons of the B-field.

In very compact sources (next lecture), $U_{\text{rad}} > U_B$ is possible, so that $P_{\text{compt}} > P_{\text{synch}}$

$\Longrightarrow$ (synchrotron) photon field will undergo dramatic amplification

$\Longrightarrow$ very efficient cooling of electrons by inverse Compton losses (Compton catastrophe).

As a result, the brightness temperature of **compact** radio sources is limited to 10^{12} K.

FR I Galaxies, I

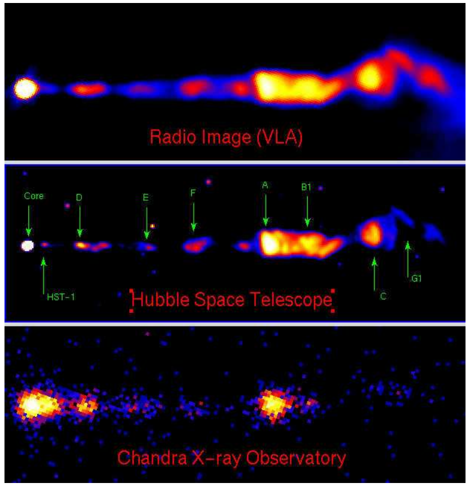

M 87 – Credit: X-ray: NASA/CXC/MIT/H.Marshall et al., Radio: F.Zhou, F.Owen (NRAO), J.Biretta (STScI), Optical: NASA/STScI/UMBC/E.Perlman et al.)

Synchrotron process dominates the broadband spectrum:

- Similar morphologies in the radio, optical, X-ray.
- X-ray spectral index α_X typically steeper than in the radio
- Correlated variability.

Electrons of energies in the range $10^7 < \gamma < 10^8$ are needed.

Common assumption:
Particle acceleration in relativistic shocks.

FR I Galaxies, II

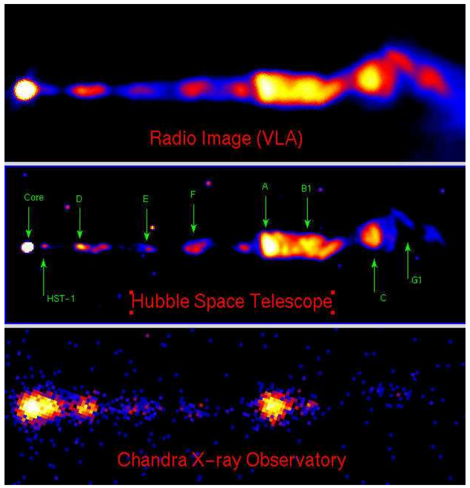

M 87 – Credit: X-ray: NASA/CXC/MIT/H.Marshall et al., Radio: F.Zhou, F.Owen (NRAO), J.Biretta (STScI), Optical: NASA/STScI/UMBC/E.Perlman et al.)

Remember Life-time of particles of energy E is

$$t_{1/2} = 1.6 \times 10^7 \text{ years} \left(\frac{B}{10^{-7}\,\text{T}}\right)^{-2} \gamma^{-1} \qquad (6.49)$$

X-ray synchrotron radiating electron of $\gamma = 10^7$ cool on time scales of years.

$\Rightarrow$ Emission regions cannot be much larger than acceleration regions.

Easy to fullfil for compact cores and even for jet knots, but continuous emission between the knots are problematic.

Electron acceleration may take place continuously, e.g., through turbulence in an outer shear layer (Stawarz & Ostrowski, 2002).

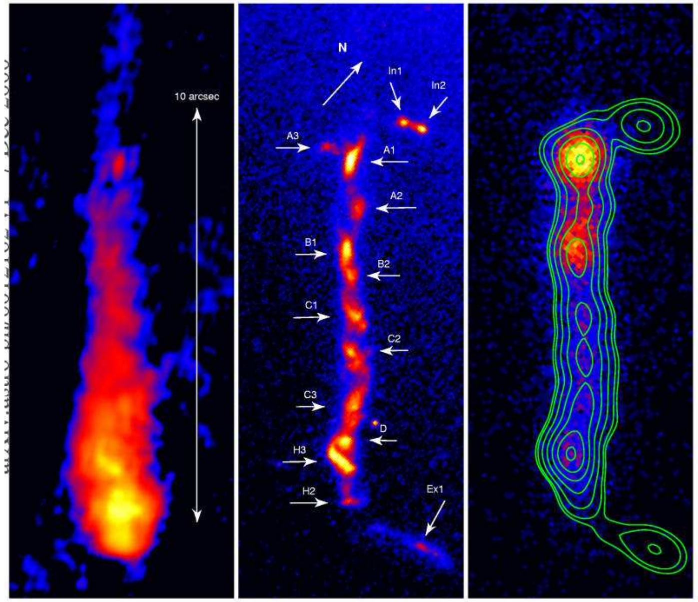

3C 273 – left: radio, 1.6 GHz (MERLIN); middle: optical, F622W filter (HST); right: X-rays, (0.5-8.0) keV (*Chandra*); (Marshall et al., 2001)

FR II Galaxies, II

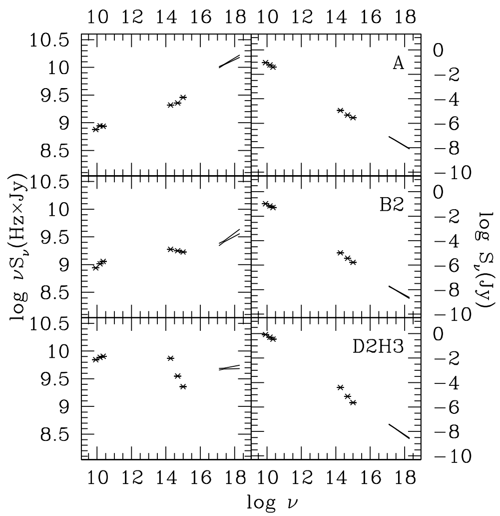

(Harris & Krawczynski, 2006)

The jet of 3C 273 is an example for the "bow-tie problem" in FR II jets: Measured X-ray spectral slopes do not permit a smooth fit with the broadband spectral data.

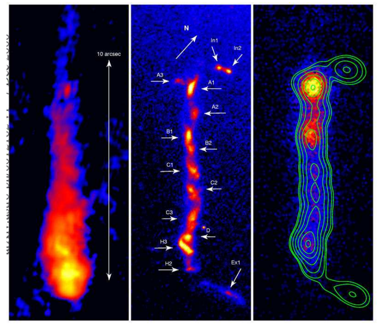

(Marshall et al., 2001)

FR II Galaxies, III

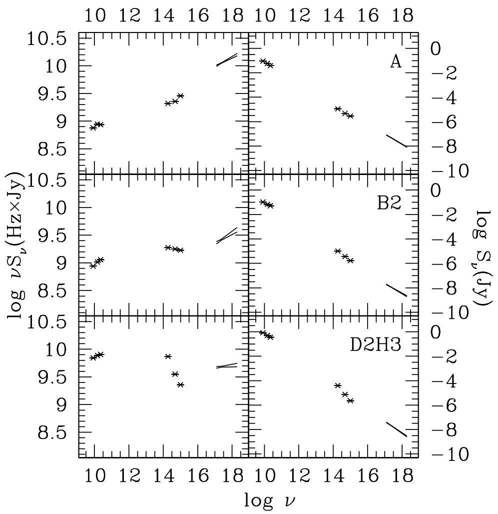

(Harris & Krawczynski, 2006)

The jet of 3C 273 is an example for the "bow-tie problem" in FR II jets: Measured X-ray spectral slopes do not permit a smooth fit with the broadband spectral data.

IC/CMB models are generally favored to explain FR II X-ray jet emission.

This is more common in FR II jets, but some FR Is have "bow-tie problems", as well.

FR II Galaxies, IV

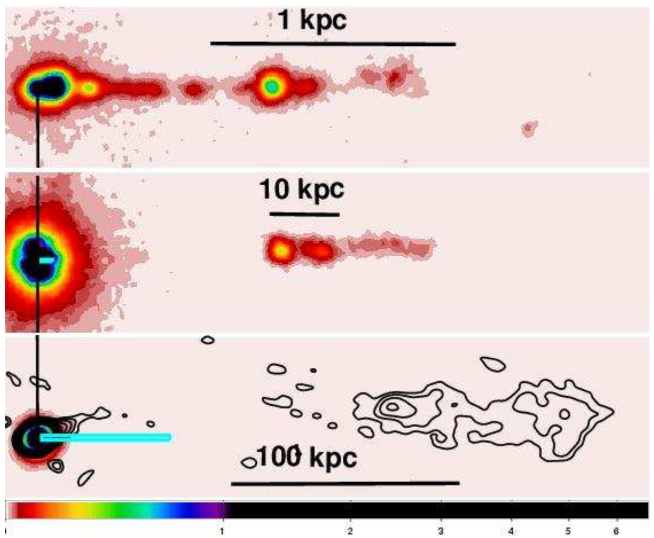

The whole jet of M 87 would easily fit into one knot of 3C 273 (Harris & Krawczynski, 2006)

FR II Galaxies, V

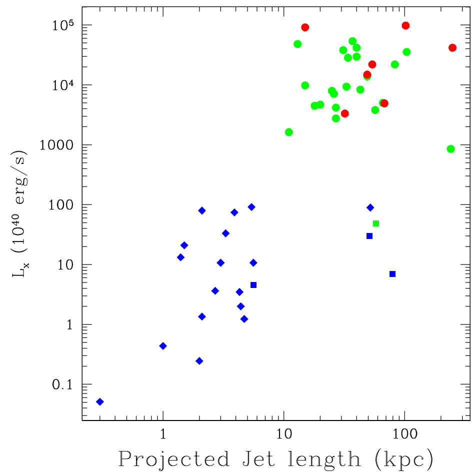

(Harris & Krawczynski, 2006) – filled circles: quasars, squares: FR IIs; diamonds: FR Is; Color code: blue: $z < 0.1$, green: $0.1 < z < 1$, red: $z > 1$.

Jet length vs. luminosity:

- Note: Plot includes beaming and projection effects
- No big surprise: quasars have powerful jets and are longer than FR I jets
- No jets between $10^{42}\,\mathrm{erg\,s^{-1}}$ and $10^{43}\,\mathrm{erg\,s^{-1}}$
- Empty upper left region: selection effect because short, distant jets are difficult to resolve
- Sparsely populated lower right region: in many cases, only inner part of FR I jets X-ray bright
- FR IIs have comparable lengths as quasars, but are weaker (beaming)

FR II Galaxies, VI

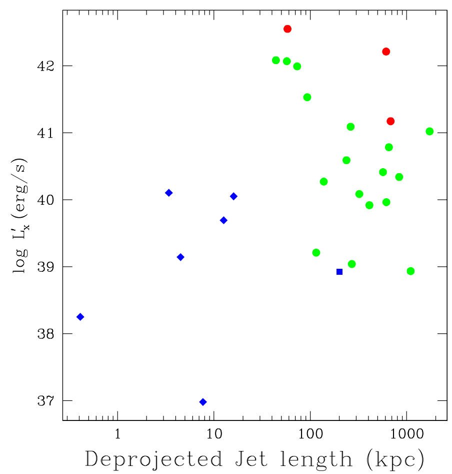

(Harris & Krawczynski, 2006) – filled circles: quasars, squares: FR IIs; diamonds: FR Is; Color code: blue: $z < 0.1$, green: $0.1 < z < 1$, red: $z > 1$.

Jet length vs. luminosity II:

- De-project and de-beam if reasonable estimates for $\mathcal{D}$ and θ exist
- Many uncertainties $\Rightarrow$ Scatter
- "Community interpretation" that FR Is are synchrotron and FR IIs IC emitters affects the luminosity axis
- Under these caveats, FR I jets and quasar jets are more clearly distinguished on the basis of size rather than luminosity
- Note that L_X denotes the jet loss, not the jet power

Relativistic Bulk Motion on Kpc Scales, I

Bulk relativistic jet motion needed on kpc scales in order to explain IC/CMB emission

- Apparent superluminal motion remains the clearest signature of bulk relativistic motion
- Well established on parsec scales with VLBI but difficult to measure on kpc scales because of a lack of sufficiently compact features
- Optical telescopes (HST) have supperior angular resolution compared to *Chandra*

Superluminal motion in M 87: (Biretta, Sparks & Macchetto, 1999)

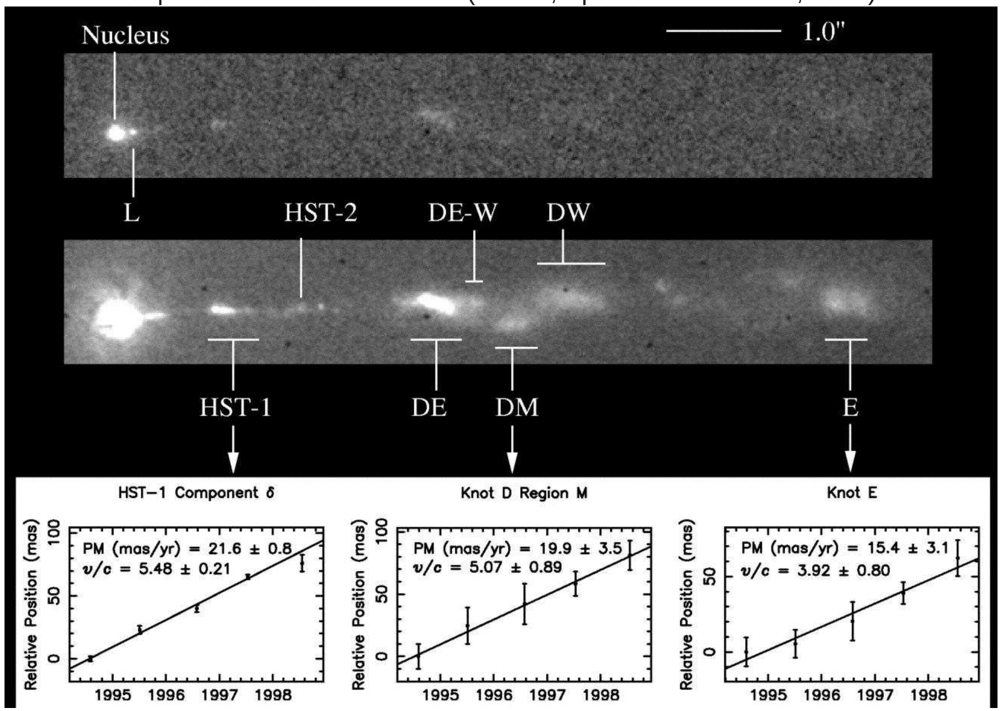

Relativistic Bulk Motion on Kpc Scales, III

Superluminal motion in M 87: (Biretta, Sparks & Macchetto, 1999)

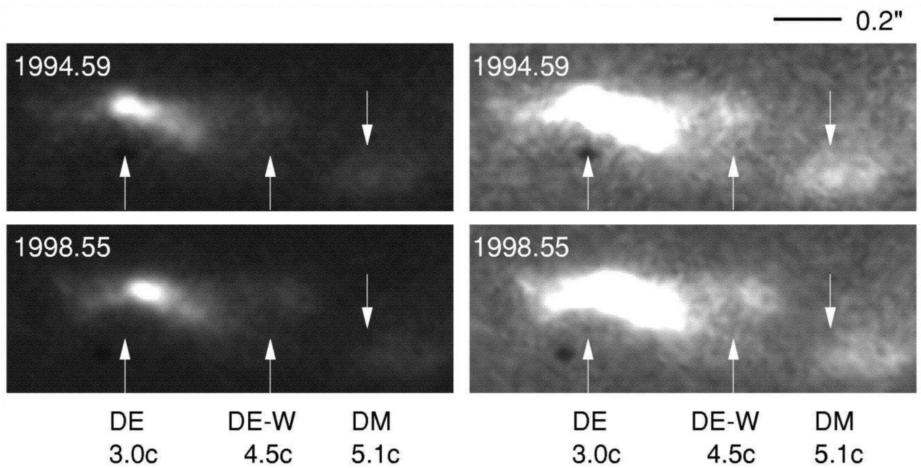

Note that MOJAVE measures only 0.05 c at 2 cm on milliarcsecond scales.

Relativistic Bulk Motion on Kpc Scales, IV

Superluminal motion in M 87: (Biretta, Sparks & Macchetto, 1999)

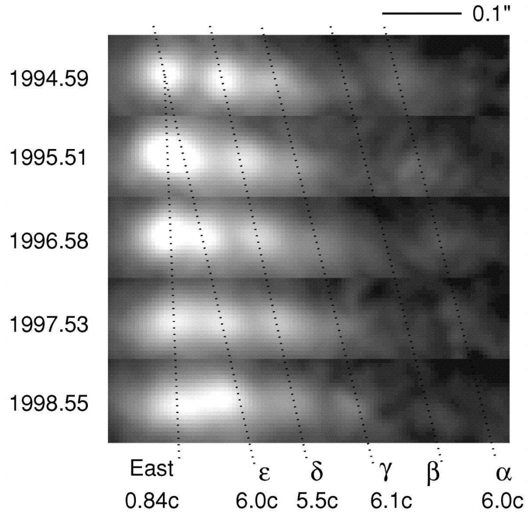

Misalignments of Radio-, Optical-, X-Ray Jet Features, I

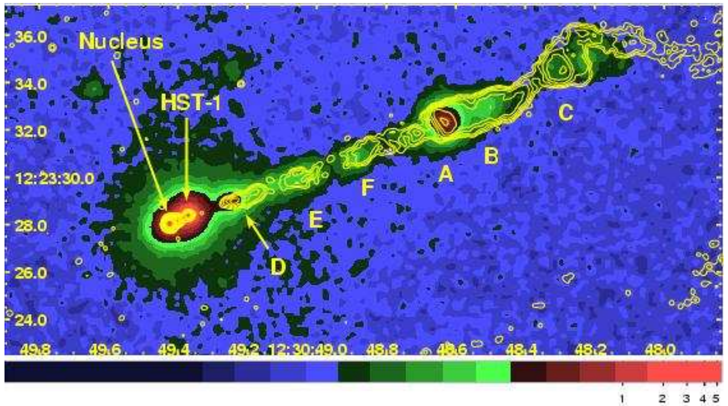

(Harris & Krawczynski, 2006)

Radio jet "circumnavigates" around an obstacle beyond knot C.
X-ray emission may come from the obstacle rather than from the jet itself.
There are offsets between radio and X-ray peaks in knots D and F.

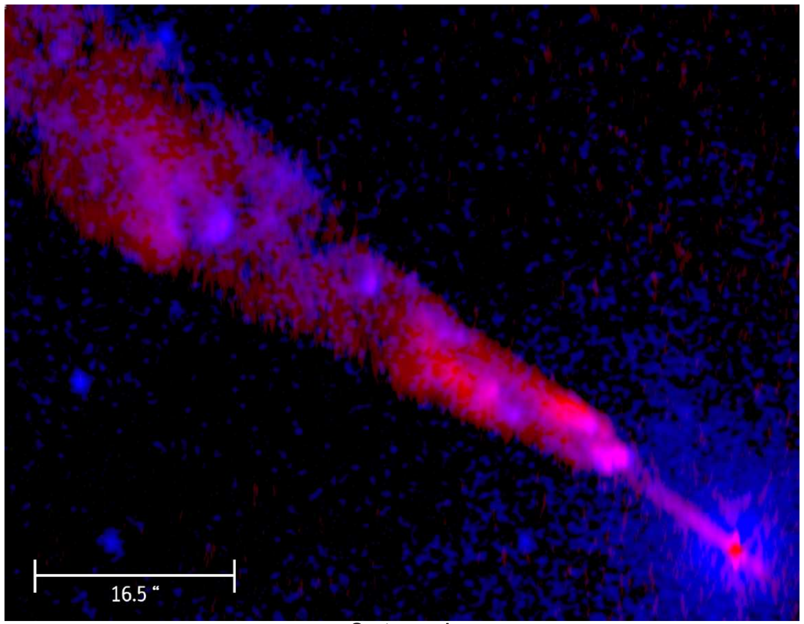

Centaurus A

Credit: X-ray: NASA/CXC/Bristol U./M. Hardcastle et al.; Radio: NRAO/AUI/NSF/Bristol U./M. Hardcastle

Misalignments of Radio-, Optical-, X-Ray Jet Features, III

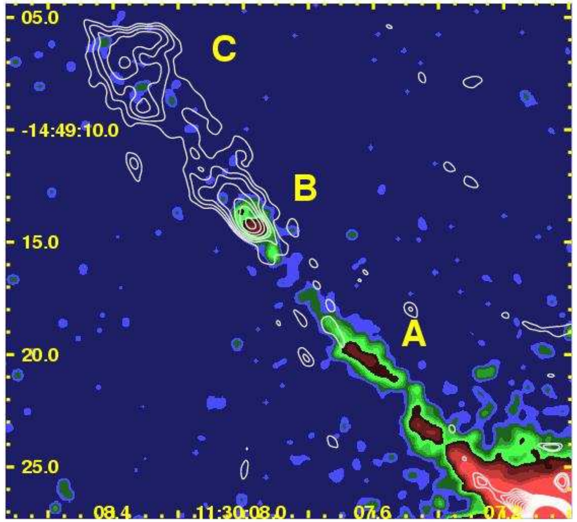

PKS 1127-145 (*Chandra*/VLA) – (Harris & Krawczynski, 2006)

- In nearby sources (Cen A, M 87), offsets are of the order of tens of parsecs
- In PKS 1127-145 ($z = 1.18$), the offset in knot B is 10 kpc.
- Resolution effects combined with radiative losses during downstream motion
- Alternatively, the radio emissivity may be enhanced downstream from a shock region
- Offsets in IC/CMB knots are much more difficult to explain

Misalignments of Radio-, Optical-, X-Ray Jet Features, IV

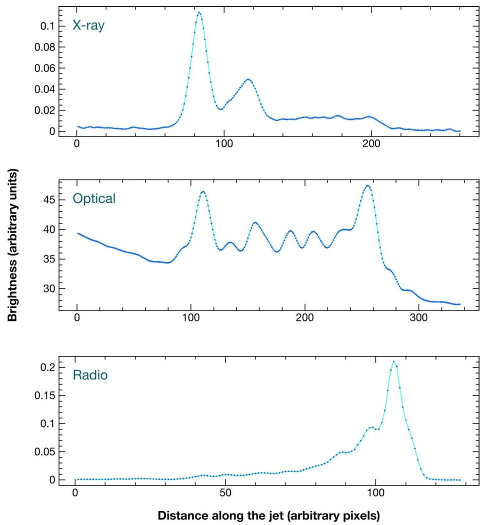

Profiles along the jet in 3C 273 – (Harris & Krawczynski, 2006)

- X-ray intensity often highest at the upstream end, whereas the radio intensity increases downstream: **Progressions**
- Common effect, most prominent in 3C 273
- Degraded angular resolution (or larger distance) would create an offset
- Progressions can be explained via increasing magnetic field strengths in synchrotron jets and via jet deceleration in IC/CMB jets.

Outlook

In IC/CMB models, the X-rays are produced from low-energy electrons from the bottom of the energy distribution. Their primary synchrotron emission would lie well below the frequencies probed until today.

Tests of synchrotron vs. IC/CMB models:

- Look for a cutoff at high X-ray energies
- Observe the IC/CMB seed-electrons in the radio: their low-frequency ($\sim$ 100 MHz) emission will be detectable with LOFAR and the LWA.
- More and deeper optical/IR observations to show if this emission is from the top end of the synchrotron spectrum or the bottom of the IC component.
- Model sensitivity of 5-yr *Fermi* all-sky survey predicts that the putative IV/CMB of many FR II knots should be detectable at GeV energies (Dermer & Atoyan, 2004); Problem: angular resolution.
- Search for signals at even higher energies (TeV range: H.E.S.S., MAGIC, VERITAS, CANGAROO); better angular resolution but; Problem: universe not transparent at high redshifts

Agudo, I., Gómez, J.-L., Martí, J.-M., Ibáñez, J.-M., Marscher, A. P., Alberdi, A., Aloy, M.-A., & Hardee, P. E., 2001, Astrophys. J., Lett., 549, L183

Biretta, J. A., Sparks, W. B., & Macchetto, F., 1999, ApJ, 520, 621

Cohen, M. H., Lister, M. L., Homan, D. C., Kadler, M., Kellermann, K. I., Kovalev, Y. Y., & Vermeulen, R. C., 2007, ApJ, 658, 232

Denn, G. R., Mutel, R. L., & Marscher, A. P., 2000, ApJS, 129, 61

Dermer, C. D., & Atoyan, A., 2004, Astrophys. J., Lett., 611, L9

Fiorucci, M., Ciprini, S., & Tosti, G., 2004, A&A, 419, 25

Harris, D. E., & Krawczynski, H., 2006, ARA&A, 44, 463

Helmboldt, J. F., Taylor, G. B., Walker, R. C., & Blandford, R. D., 2008, ApJ, 681, 897

Lind, K. R., & Blandford, R. D., 1985, ApJ, 295, 358

Marshall, H. L., et al., 2001, Astrophys. J., Lett., 549, L167

Marshall, H. L., et al., 2005, ApJS, 156, 13

Pearson, T. J., & Readhead, A. C. S., 1981, ApJ, 248, 61

Pearson, T. J., & Readhead, A. C. S., 1988, ApJ, 328, 114

Polatidis, A. G., Wilkinson, P. N., Xu, W., Readhead, A. C. S., Pearson, T. J., Taylor, G. B., & Vermeulen, R. C., 1995, ApJS, 98, 1

Sambruna, R. M., Gambill, J. K., Maraschi, L., Tavecchio, F., Cerutti, R., Cheung, C. C., Urry, C. M., & Chartas, G., 2004, ApJ, 608, 698

Stawarz, Ł., & Ostrowski, M., 2002, ApJ, 578, 763

Taylor, G. B., et al., 2007, ApJ, 671, 1355

Thakkar, D. D., Xu, W., Readhead, A. C. S., Pearson, T. J., Taylor, G. B., Vermeulen, R. C., Polatidis, A. G., & Wilkinson, P. N., 1995, ApJS, 98, 33

Xu, W., Readhead, A. C. S., Pearson, T. J., Polatidis, A. G., & Wilkinson, P. N., 1995, ApJS, 99, 297